
MM-Fi: Multi-Modal Non-Intrusive 4D Human Dataset for Versatile Wireless Sensing

Jianfei Yang^{1*}, He Huang¹, Yunjiao Zhou¹, Xinyan Chen¹, Yuecong Xu¹,
Shenghai Yuan¹, Han Zou¹, Chris Xiaoxuan Lu², Lihua Xie¹

¹School of Electrical and Electronic Engineering, Nanyang Technological University

²School of Informatics, University of Edinburgh

Project Page: <https://ntu-aiot-lab.github.io/mm-fi>

Dataset Toolbox: https://github.com/ybhbingo/MMFi_dataset

Abstract

4D human perception plays an essential role in a myriad of applications, such as home automation and metaverse avatar simulation. However, existing solutions which mainly rely on cameras and wearable devices are either privacy intrusive or inconvenient to use. To address these issues, wireless sensing has emerged as a promising alternative, leveraging LiDAR, mmWave radar, and WiFi signals for device-free human sensing. In this paper, we propose MM-Fi, the first multi-modal non-intrusive 4D human dataset with 27 daily or rehabilitation action categories, to bridge the gap between wireless sensing and high-level human perception tasks. MM-Fi consists of over 320k synchronized frames of five modalities from 40 human subjects. Various annotations are provided to support potential sensing tasks, *e.g.*, human pose estimation and action recognition. Extensive experiments have been conducted to compare the sensing capacity of each or several modalities in terms of multiple tasks. We envision that MM-Fi can contribute to wireless sensing research with respect to action recognition, human pose estimation, multi-modal learning, cross-modal supervision, and interdisciplinary healthcare research.

1 Introduction

Human sensing and modeling serve as the fundamental technology in computer vision, human-computer interaction, ubiquitous computing, and computer graphics [16]. Accurately recognizing human activities and reconstructing human pose empower a broad spectrum of applications, *e.g.*, gaming, home automation, autonomous driving, augmented and virtual reality, animation, and rehabilitation. However, existing methods mainly rely on cameras [25] and wearable inertial sensors [50], where significant limitations exist when applied in real-world scenarios. For instance, cameras result in privacy concerns in domestic settings and are susceptible to lighting conditions. Wearable inertial sensors are low-cost solutions but require strong user compliance for wearing them at all time.

Recently, wireless human sensing has emerged as a promising solution that leverages non-intrusive sensors such as LiDAR, mmWave radar, and WiFi to address the limitations of illumination, privacy, and inconvenience [27]. These device-free sensors spread laser or radio frequency (RF) signals whose responses reflect human motions in different levels of granularity: high-resolution point cloud data from LiDAR [21], medium-resolution point cloud from mmWave radar [2], and low-resolution channel state information (CSI) from WiFi [47, 56]. These data modalities are complementary to existing camera-based or device-based solutions and enable more privacy-preserving human sensing applications such as homes and hospitals.

In this work, we present **MM-Fi**, a multi-modal non-intrusive 4D (spatial-temporal) human dataset for high-fidelity human sensing to facilitate the algorithm development of wireless human sensing.

*Corresponding authors (yang0478@e.ntu.edu.sg)

MM-Fi consists of 1080 consecutive sequences with over 320k synchronized frames from five sensing modalities: RGB image, depth image, LiDAR point cloud, mmWave radar point cloud, and WiFi CSI data. The dataset includes annotations for 2D/3D human pose landmarks, action categories, 3D human position, and estimated 3D dense pose. To the best of our knowledge, MM-Fi is the first dataset that comprises five non-intrusive modalities for 4D human pose estimation (HPE). The contributions and features of MM-Fi are listed below.

Multiple Sensing Modalities. MM-Fi contributes to multimodal human sensing by considering the potentially complementary nature of different sensing modalities. MM-Fi provides five non-intrusive sensing modalities including RGB frames, depth frames, LiDAR point cloud, mmWave radar point cloud, and WiFi CSI data, with kinds of annotations, *i.e.*, 2D pose landmarks of an RGB camera and stereo camera, 3D pose landmark, action category, and 3D human position.

Synchronized Mobile Sensor Platform. MM-Fi is collected by a novel customized platform that captures and synchronizes multiple sensors through a mini-PC running the Robot Operating System (ROS). The mobility of our platform enables us to collect data in diverse environments.

Profuse Action Sets. MM-Fi consists of 27 categories of human actions including 14 daily actions and 13 clinically-suggested rehabilitation actions. Therefore, MM-Fi can contribute to ubiquitous computing, *e.g.*, home automation applications, and healthcare research, *e.g.*, the evaluation and recovery of neuroscience disorders or physical body injury.

Versatile Sensing with Unexplored Tasks. The rich variety of data modalities and annotations in MM-Fi enables diverse sensing tasks, such as multi-modal fusion and cross-modal supervision for human sensing. Furthermore, MM-Fi opens up new research possibilities for previously unexplored tasks, *e.g.*, human pose estimation using the combinations of two or three sensor modalities, and unexplored problems, *e.g.*, domain generalization in wireless multi-modal sensing.

Extensive Benchmarks. To facilitate future research, we release the pre-processed dataset, various annotations, the codes for data loading, and extensive benchmarks on multi-modal human pose estimation and skeleton-based action recognition.

2 Related Work

2.1 Human Pose Estimation

3D human pose estimation has been extensively studied with the deployment of various sensing schemes including marker-based sensing and marker-less sensing, in which the marker-less sensing is more widely accepted for its non-intrusive and user-friendly properties [37, 40, 2, 3, 7, 14, 36, 46]. Vision-based approaches take over the majority of 3D HPE owing to the popularity of cameras, where the 2D keypoints are usually recognized from RGB frames and a deep learning model will be proposed to generate 3D joints based on a set of 2D keypoints [37]. As a result, RGB and depth cameras are also included in our dataset. Though RGB cameras produce high-resolution images, they suffer in poor lighting conditions and are fragile to weather conditions [7]. Depth cameras are capable of providing dense point clouds with the texture of human body, but they still face the problems of high noise and outliers [21]. For more stable and accurate sensing, we also consider exploring LiDAR for 3D HPE in this dataset, which is previously applied in industrial fields such as SLAM and autonomous driving [54]. Compared with cameras, LiDAR is more robust to noise and thus obtains more reliable human body texture [21]. Also, the cost of LiDAR devices is gradually falling as a result of the recent laser technology development. However, it would also be affected by occlusion, which makes the point cloud texture less representative. Despite the accuracy, LiDAR is still expensive for many scenarios and only realistic for a limited amount of applications. Besides vision-based sensing, radio frequency sensing is a promising technique for 3D HPE [52, 27]. mmWave-based HPE has been paid increasing attention thanks to the comparable performance to vision-based approaches and the privacy-concerned merit [36, 1]. Thus, mmWave is exploited in our dataset. In addition to mmWave-based sensing, WiFi CSI-based sensing is also emerging recently. WiFi sensing has been reported in several applications (*e.g.*, respiratory monitoring, gesture, and action recognition.) but is seldom seen for 3D HPE [58, 57, 46]. Now, our dataset includes WiFi sensing for related research. Furthermore, the obtained 3D human poses can be applied to realize action recognition tasks.

Dataset	Modalities					Annotations				# Subj	# Act	# Seq	# Frame
	RGB	Depth	LiDAR	mmWave	WiFi	Action	3DPOS	2DKP	3DKP				
COCO [23]	✓	-	-	-	-	-	-	✓	-	-	-	-	104k
MPII [4]	✓	-	-	-	-	✓	-	✓	-	-	-	410	24k
MPI-INF-3DHP [24]	✓	-	-	-	-	-	-	✓	✓	-	-	8	16
CMU Panoptic [18]	✓	✓	-	-	-	-	-	✓	✓	-	-	8	65
Human3.6M [16]	✓	✓	-	-	-	✓	-	✓	✓	-	-	11	839
NTU RGB+D [37]	✓	✓	-	-	-	✓	-	✓	✓	-	-	40	56k
3DPW [40]	✓	-	-	-	-	-	-	✓	✓	-	-	7	60
MPI08 [30]	✓	-	-	-	-	-	-	-	✓	-	-	4	24
TNT15 [41]	✓	-	-	-	-	✓	-	-	✓	-	-	1	5
MoVi [14]	✓	-	-	-	-	✓	-	✓	✓	-	-	90	21
LiDARCap [21] *	✓	-	✓	-	-	✓	-	-	✓	-	-	13	20
LIPD [34] *	✓	-	-	-	-	✓	-	-	-	-	-	15	30
LiCamPose [10] *	✓	-	✓	-	-	✓	-	-	✓	-	-	-	6
SLOPER4D [11]	✓	-	✓	-	-	-	-	-	-	-	-	12	15
CIM4D [45]	✓	-	✓	-	-	-	-	✓	✓	-	-	12	42
Waymo [54] *	✓	✓	✓	-	-	-	-	✓	✓	-	-	13	1950
HuMMan [7]	✓	✓	✓	-	-	✓	-	✓	✓	-	-	1000	500
RF-Pose [52] *	✓	-	-	✓	-	✓	-	✓	-	-	-	100	1
RF-Pose3D [53] *	✓	-	-	✓	-	✓	-	✓	✓	-	-	>5	5
mmPose [36] *	-	-	-	✓	-	✓	-	-	✓	-	-	2	4
mmMesh [44] *	✓	-	-	✓	-	✓	-	-	✓	-	-	20	8
MARS [2]	-	-	-	✓	-	✓	-	-	✓	-	-	4	10
mmBody [8]	✓	✓	-	✓	-	✓	-	-	✓	-	-	20	100
mRI [1]	✓	✓	-	✓	-	✓	-	✓	✓	-	-	20	12
AHA-3D [5]	✓	-	-	-	-	✓	-	-	✓	-	-	21	4
HPTE [6]	✓	✓	-	-	-	✓	-	-	✓	-	-	5	8
WiPose [17] *	✓	-	-	-	✓	✓	-	-	✓	-	-	10	16
GoPose [33] *	✓	-	-	-	✓	✓	-	-	✓	-	-	10	>9
MM-Fi	✓	✓	✓	✓	✓	✓	✓	✓	✓	✓	✓	40	27
												1080	320.76k

Table 1: Comparisons of MM-Fi with published datasets. * denotes that the dataset is not accessible. The proposed MM-Fi includes all five non-intrusive sensors, and has four types of annotations including action category (Action), 3D subject position (3DPOS), 2D and 3D whole-body keypoints (2DKP and 3DKP), and 3D dense pose (3DDP). Compared to existing RGB-D datasets, MM-Fi has more sensor modalities and various annotations.

2.2 Multi-modal Human Dataset

With the emergence of applications to human pose estimation, multi-modal datasets with annotations will strongly support the research in relevant fields. Previously published datasets on HPE and our dataset are summarized and compared in Table 1. Traditional datasets on HPE mainly rely on RGB or depth frames, which provide 2D or 3D keypoints as the ground truth (*e.g.*, COCO [23], NTU RGB+D [37]). Recent works on radio frequency-based HPE apply mmWave (some assisted with RGB images) as the sensing modality (*e.g.*, mmPose [36], RF-Pose3D [53] with RGB). Waymo [54] and HuMMan [7] are the popular choices for LiDAR-based HPE algorithms development. In addition, with the increasing attention in WiFi sensing field, datasets with WiFi sensory inputs have been published for pose estimation with 3D annotations and action labels (*e.g.*, WiPose [17], GoPose [33]). Despite the development of the aforementioned works, there is still much room for HPE dataset. First, the mentioned datasets [23, 37, 36, 2, 17] support no more than three non-intrusive modalities, making it difficult to develop multi-modal sensing systems. Second, the quantity of most datasets related to mmWave and WiFi sensing is not sufficient in both the number of subjects and actions and the domain settings, which can impact the performance of wireless sensing. While recent works such as the mRI dataset [1] have made promising progress by supporting multiple modalities, including maker-based and maker-less sensing techniques (*i.e.*, IMU, RGB, depth and mmWave), the aforementioned challenges still remain due to the lack of LiDAR and WiFi modalities and multiple domains. To address these challenges, our MM-Fi emphasizes the diversity of modalities and the variety of domain settings. Meanwhile, our dataset is equipped with richer data content in comparison to the majority of the above datasets (both in the number of subjects and actions). To the best of our knowledge, the MM-Fi is the first 3D HPE dataset with most of the non-intrusive sensing modalities, including RGB, depth, LiDAR, mmWave, and WiFi [15, 35], and with multiple kinds of annotations. MM-Fi thus has the potential to contribute to various research tasks in machine learning, computer vision, ubiquitous computing, and healthcare.

3 Sensor Platform

To facilitate data collection for our MM-Fi dataset, we develop a customized sensor platform that consists of the Intel RealSense D435 camera, the Texas Instrument IWR6843 60-64GHz mmWave

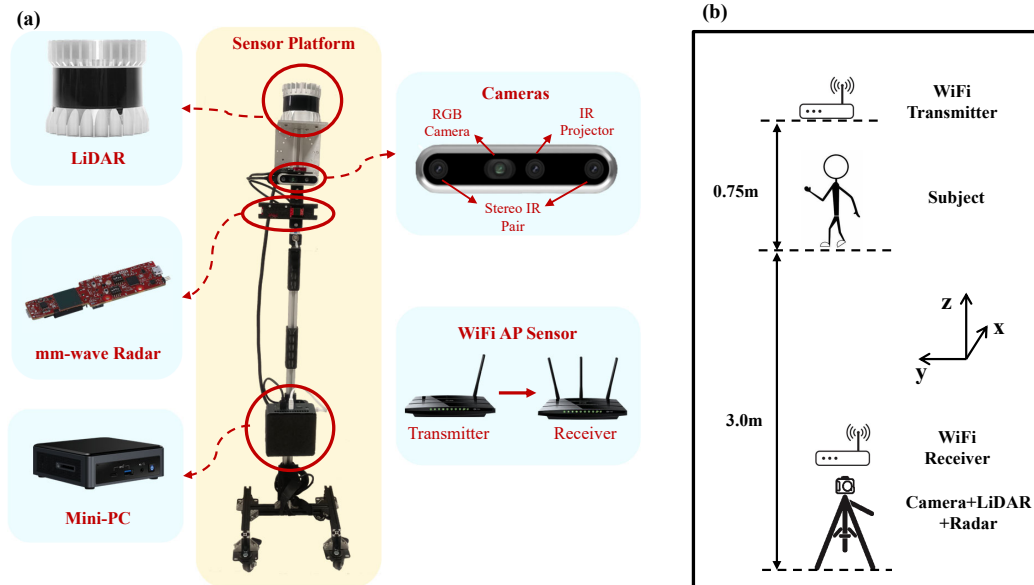


Figure 1: Overview of the experimental setup for data collection. (a) shows the customized sensor platform with one mini-PC for data synchronization and four sensor devices including Ouster OS1 32-channel LiDAR, TI IWR6843 mmWave radar, Intel Realsense D435 stereo depth camera, and TP-Link N750 WiFi APs. (b) shows the layout of data collection where all subjects are positioned 3.0m away from the platform. The WiFi transmitter is placed 0.75m away from the subject.

radar, the Ouster OS1 32-line LiDAR, and a pair of TP-Link N750 WiFi APs. As shown in Figure 1, all the sensors and one mini-PC are integrated into a mobile platform with ROS installed on the mini-PC for data collection and synchronization, with the platform placed 3.0 meters away from the subject during data collection. The features of these sensor modalities are compared in Table 2.

3.1 Sensor Modalities

RGB-D Frames from Cameras. We utilize an Intel Realsense D435 stereo depth camera to capture RGB-D frames. The camera consists of one high-precision RGB camera and two infra-red cameras with the resolutions of 1920×1080 and 1280×720 , respectively. We calibrate the three cameras and consider the center of the RGB camera as the origin of the world coordinate system.

Point Cloud from Radar and LiDAR. Our point cloud data is obtained using a Texas Instruments (TI) IWR6843 mmWave radar and an Ouster OS1 32-channel LiDAR. The LiDAR point clouds are dense and cover the full range of human movement, with each LiDAR point P_l represented by the spatial coordinates $P_l = (x, y, z)$. In contrast, the IWR6843 mmWave radar generates more sparse point clouds by emitting Frequency Modulated Continuous Waves (FMCW), which vary the frequency of the transmitted signal by a modulating signal at a known rate over a fixed time period. The reflected signals are used to measure the frequency difference and Doppler frequency for computing the distance and the speed of an object respectively. In this manner, a single point in a mmWave radar point cloud is represented as $P_m = (x, y, z, d, I)$, where (x, y, z) indicates the spatial coordinates, d denotes the Doppler velocity, and I denotes the signal intensity. It is found that the number of points in one frame is too small for mmWave radar and sometimes the empty frame may appear due to the hardware instability. To address this issue, we aggregate each mmWave frame using the adjacent frames within its consecutive 0.5s period to increase the number to around 128. This strategy has been previously proposed in radar-based human pose estimation method [3].

WiFi CSI Data. WiFi CSI data describes the propagation link from the transmitter to the receiver. Recent studies have shown human movements can affect the CSI data extracted from WiFi signals, enabling WiFi-based human sensing which is ubiquitous, privacy-preserving, and cost-effective [46]. For WiFi CSI data collection, we built the WiFi sensing system [48] based on two Commercial Off-The-Shelf (COTS) WiFi Access Points, TP-Link N750, and the Atheros CSI Tool [43]. The platform

Modality	Rate	Freq.	Privacy	Illum.	Range	Granularity	Cost	Data
RGB	30Hz	-	*	*	**	***	**	RGB frame
Depth	30Hz	-	**	**	**	**	**	Depth and infra-red frame
LiDAR	20Hz	360THz	***	***	***	***	***	Point cloud
mmWave	30Hz	60-64GHz	***	***	***	**	**	Sparse point cloud
WiFi	1000Hz	5GHz	***	***	*	*	*	CSI frame

Table 2: Comparisons of five non-intrusive sensors. Rate: Sampling rate. Freq.: Signal frequency. Privacy: privacy-preserving ability. Illum.: Robustness to illumination. Range: Sensing range. Resolution: Data resolution. Cost: cost of sensors.

runs at 5GHz with a bandwidth of 40MHz, enabling the collection of CSI data with 114 subcarriers per pair of antennas at up to a sampling rate of 1000Hz. As shown in Figure 1, we embedded the receiver with three antennas on the sensor platform, and the transmitter with one antenna is placed on the other side. For the smoothness and stability of CSI data, we have implemented the average sliding window method inside the firmware of the sensing platform, which could produce a CSI stream of about 100Hz. Besides, due to the inconsistency of data acquisition rate between different modalities, the CSI data is further augmented to form a $3 \times 114 \times 10$ matrix within a time period of 100ms.

3.2 Synchronization

Synchronization is an indispensable prerequisite for a multi-modal human dataset. To achieve synchronization, we connect all the sensors and the WiFi receiver to the same mini-PC and develop a data collection system using the Robot Operating System (ROS) [31]. In ROS, all the sensor modalities are saved in a ROS bag with the timestamp at each frame. According to the sampling timestamp, we set a 10Hz sampling timestamp and retrieve the multi-modal data frames that are closest to this timestamp. In this manner, we guarantee that the collected data are well-synchronized, with the synchronization error being within 25ms as the lowest sampling rate of all sensors is 20Hz (LiDAR).

4 Dataset

4.1 Subjects

Our human subject study is approved by the IRB at the Nanyang Technological University. The subject recruitment is voluntary, and the involved subject has been informed that the de-identified data was made publicly available for research purposes. The recruitment process is voluntary, and the experiments are conducted in several labs. Prior to participation, we provide detailed information to the subjects about the research goal, data collection procedure, potential risks, and the tutorial. The consent form is signed by every participating subject. Eventually, we recruit 40 human subjects locally in the university including 11 females and 29 males, with an average age of 25.3 ± 2.8 , weight of 66.1 ± 12.0 kg, height of 172.3 ± 7.9 cm, and Body Mass Index (BMI) of 22.2 ± 3.2 .

4.2 Categories of Human Motions

MM-Fi consists of 27 action categories which include 14 daily activities and 13 rehabilitation exercises. The daily activities are geared towards potential smart home and building applications, while the rehabilitation categories are designed to contribute to healthcare applications. Specifically, the daily activities include the common physical activities of various body parts: (a) chest expanding horizontally, (b) chest expanding vertically, (c) left side twist, (d) right side twist, (e) raising left arm, (f) raising right arm, (g) waving left arm, (h) waving right arm, (i) picking up things, (j) throwing toward left side, (k) throwing toward right side, (l) kicking toward left direction using right leg, (m) kicking toward right direction using left leg, (n) bowing. Meanwhile, the rehabilitation exercises are derived from [1] as (a) stretching and relaxing in free form, (b) mark time, (c) left upper limb extension, (d) right upper limb extension, (e) left front lunge, (f) right front lunge, (g) both upper limbs extension, (h) squat, (i) left side lunge, (j) right side lunge, (k) left limbs extension, (l) right limbs extension, (m) jumping up. These exercises are known to relieve pain, light up mood and reduce anxiety and fatigue. Each subject performs all 27 actions for a duration of 30 seconds.

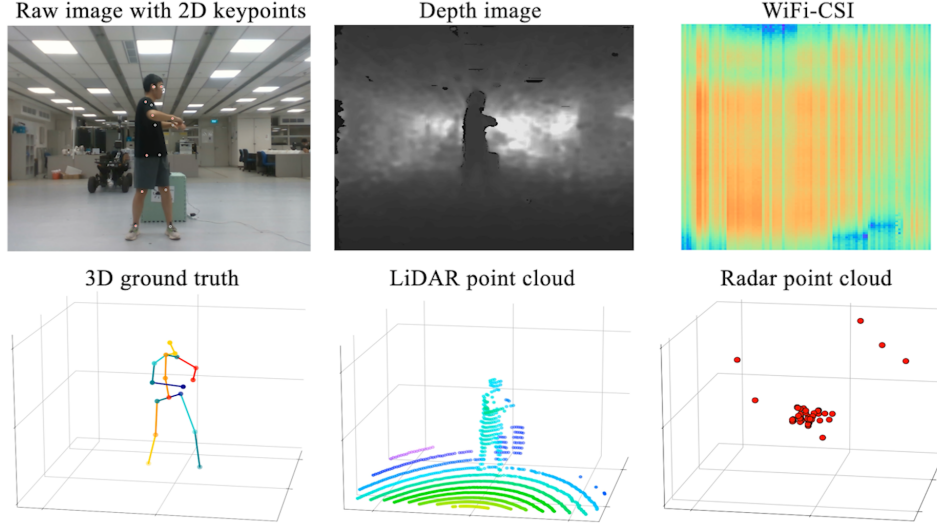


Figure 2: The visualization of five sensor modalities and 3D annotation in MM-Fi.

4.3 Data Annotation and Processing

2D and 3D Human Pose Annotation. We start by utilizing a large deep learning model, HRNet-w48 [39], to obtain the 2D keypoints $\mathcal{K}_{2D} = \{k_i \in \mathbb{R}^{17 \times 2}, i = 1, \dots, N\}$ of N frames from the two views, *e.g.*, two infra-red cameras. Then relying on the intrinsic and extrinsic parameters of cameras derived from the camera calibration, we triangulate 3D keypoints $\hat{\mathcal{P}}_{3D} = \{p_i \in \mathbb{R}^{17 \times 3}, i = 1, \dots, N\}$ with the two views of 2D keypoints. However, due to the possibility of inaccurate triangulation, we further refine the 3D keypoints through an optimization process, which can be generally described as:

$$\min_{\hat{\mathcal{P}}_{3D}} \mathcal{L} = \mathcal{L}_G + \lambda_0 \mathcal{L}_A, \quad (1)$$

$$\mathcal{L}_G = \sum_{n=1}^N \left\{ \lambda_1 \sum_{c=1}^C \|f_c(p_n) - k_n^c\| + \lambda_2 \|p_{n+1} - p_n\| + \lambda_3 \sum_{j \in \Omega_B} \|\mathcal{B}_{n,j} - \bar{\mathcal{B}}_j\| \right\}, \quad (2)$$

where \mathcal{L}_G and \mathcal{L}_A denote the general regularizer and action regularizer, respectively. In \mathcal{L}_G , the function $f_c(\cdot)$ projects the world coordinate to the pixel coordinate of the c th camera, parameterized by the corresponding intrinsic matrix, distortion coefficients and rotation-translation matrices. The first term of the loss function denotes the reprojection error of all C cameras. The second term represents the smoothness loss that is introduced to reduce inter-frame outliers [1]. Moreover, for a specific subject, the bone (*e.g.*, leg) length $\{\mathcal{B}_j\}$ should remain constant regardless of the action, we thus apply a bone length constraint to the optimization process, where Ω_B and $\bar{\mathcal{B}}_j$ denote the bone indices collection and the average length of j th bone for all frames [7] respectively. The triangulated 3D keypoints $\hat{\mathcal{P}}_{3D}$ serve as the initial value, and after optimization, we obtain $\hat{\mathcal{P}}_{3D} \rightarrow \mathcal{P}_{3D}$, which is considered as the ground truth for 3D keypoints. However, purely minimizing \mathcal{L}_G does not optimize the estimated 3D joints well. For example, actions with turn-back and crouch may have occlusion, leading to incorrect recognition of some keypoints in the observed data regardless of the type of sensor utilized. Therefore, we set limitations on some joints based on the actions and bone lengths, which is why we introduce the action regularizer \mathcal{L}_A . The formation of \mathcal{L}_A depends on the specific action and is described in the Appendix A.2.

3D Position. For mmWave radar and WiFi, an essential task is to estimate the precise 3D position of a subject with respect to the sensor, which serves many applications such as gaming and metaverse avatar simulation. To this end, we propose to additionally fuse the results of LiDAR data point and camera to provide the circumscribed cube of the subject. We annotate 2000 frames randomly sampled from MM-Fi to validate that the average error of the 3D position cube is within 50 mm.

3D Dense Pose. Recently, 3D human body modeling arouses more attention for AR and metaverse applications [20]. Dense pose estimation aims at mapping sensing data to the 3D surface of the human body [15], which is currently achieved by RGB. To enable wireless dense pose estimation based on radar, LiDAR, and WiFi, we provide the labels obtained from an advanced RGB-based dense estimation model [26] utilized in recent work for pose annotation [13].

Temporal Action Segments. Temporal action segmentation aims at densely identifying actions in long RGB sequences, and has become an increasingly essential task thanks to the growing numbers of long videos [12, 22, 42, 19]. Currently, temporal action segmentation is achieved through RGB. To enable temporal action segmentation based on modalities other than RGB (i.e., radar, LiDAR, and WiFi) and to provide more fine-grained samples, we provide the temporal segment labels obtained through a comprehensive segment annotation process. The details of the annotation process and annotation samples are presented in the Appendix.

Post-Processing and Data Loader. We unify the coordinate system for the point cloud data from LiDAR and mmWave radar according to the right-hand rule. To ensure the synchronized frame for all modalities, we construct the frame of MM-Fi dataset with a uniform sampling rate of 10Hz. Figure 2 shows one MM-Fi data frame. All the data except the temporal segments are saved using the *numpy* array format, i.e., “*np*” files, while the temporal segments are saved using a single “.*csv*” file. The PyTorch data loader is provided to load one or multiple modalities conveniently.

Keypoints Quality To evaluate the quality of our 3D keypoints, we first re-project them onto 2D keypoints and then manually annotate 100 frames for each action category, resulting in a total of 2,700 video frames. We compute the re-projection error as the percentage of correctly located keypoints using a threshold of 50% of the head segment length (denoted as PCKh@0.5). The analysis reveals that the re-projection PCKh@0.5 is 95.66%, indicating the high quality of our annotation.

Intended Uses MM-Fi opens up a wide range of applications in human sensing tasks, encompassing both existing and novel areas. By harnessing diverse modalities, it facilitates robust 2D/3D human pose estimation (HPE) across various modalities, paving the way for multi-sensor HPE through effective multi-modal learning techniques. Moreover, due to the inclusion of multiple subjects and environments, MM-Fi empowers new sensing and recognition tasks in wireless sensing. It enables self-supervised multi-modal sensing, revolutionizing the way data is leveraged across different modalities without relying on explicit annotations. MM-Fi empowers cross-domain HPE by developing new domain adaptation and domain generalization techniques, contributing to pose estimation across different domains and environments. Lastly, it enables few-shot action recognition by providing a rich dataset encompassing various actions and scenarios, empowering efficient and accurate recognition of actions with limited training samples. The versatility and richness of MM-Fi make it a valuable resource for researchers and practitioners in the field of human sensing.

5 Benchmark and Evaluation

In this section, we introduce the benchmark setup, evaluation metrics, and baseline methods for single-modal and multi-modal human pose estimation based on the proposed MM-Fi dataset. The results are analyzed to show the merits and drawbacks of these modalities. We also include a benchmark on skeleton-based action recognition [38, 9] using our dataset as a supplement in the Appendix.

5.1 Benchmark Setup

Protocol. We provide three protocols that are tailored to the various scenarios, based on the categories in Section 4.2. **Protocol 1 (P1)** includes 14 daily activities that are performed freely in space, e.g., picking up things and raising arms. **Protocol 2 (P2)** includes 13 rehabilitation exercises that are performed in a fixed location, e.g., limb extension. **Protocol 3 (P3)** includes all 27 activities. By using these three protocols, we evaluate the performance of the models on both free and fixed actions.

Data Splits. To evaluate the model, we provide three data split strategies. **Setting 1 (S1 Random Split)** involves a random split of all video samples into training and testing sets, with a split ratio of 3:1. **Setting 2 (S2 Cross-Subject Split)** splits the data by subject with 32 subjects for training and 8 subjects for testing. **Setting 3 (S3 Cross-Environment Split)** randomly selects 3 environments for training and 1 environment for testing.

Evaluation Metrics. We assess the performance of the models using two widely-used metrics in human pose estimation: Mean Per Joint Position Error (MPJPE) and Procrustes Analysis MPJPE (PA-MPJPE) [16]. MPJPE measures the difference between the ground truth and prediction for all joints by Euclidean distance after aligning the pelvis of the estimated and true 3D pose. PA-MPJPE refers to the MPJPE after adopting the Procrustes method [55] for alignment, which conducts a similarity transformation including translation, rotation, and scaling before the MPJPE calculation. MPJPE measures both the quality of joints and the spatial position, while PA-MPJPE focuses on the quality of joints. We provide the mean and standard deviation of these metrics across 3 runs.

Baseline Methods. We evaluate the model of 3D human pose estimation using a single modality including RGB image (I), LiDAR (L), mmWave radar (R), and WiFi (W) using the recent models. These methods are briefly introduced as follows:

- **RGB:** We use the RGB-based pose estimation model from [29] that transforms a sequence of 2D keypoints into 3D pose using a convolutional neural network. In the benchmark, we directly use its pre-trained model and evaluate it on our test sets.
- **LiDAR and mmWave:** For mmWave radar, we adopt the data processing technique from [2] that aggregates the consecutive frames into one data sample, while we directly use the vanilla LiDAR point cloud at each frame. Then we upgrade the neural network in [2] using the PointTransformer [51]. The model is trained from scratch using our training split.
- **WiFi:** We employ the data processing and model from MetaFi++ [56] with a convolutional network and some transformer blocks trained to regress WiFi CSI data to a root joint. The model is trained from scratch on our dataset.

We evaluate the performance of combining multiple modalities for various scenarios, including a robotics setting (I+L), low-cost setting (R+W), privacy-preserved setting (R+L+W), and all modality fusion (R+L+W+I). We adopt the simple result fusion method in the benchmark following the Least Mean Square (LMS) algorithm to learn the fusion weights of multiple sensors through linear combination [28] and leave space for future multi-modal fusion research. Instead of directly solving for the optimal weighting coefficients for each sensor, we reformulate the problem as a search for the optimal mean square estimation error, which allows for automatic parameter adjustment without the need for a correlation matrix.

5.2 Results and Analytics

Random Split Results (S1). Table 3 presents the evaluation results for human pose estimation using a single modality, including RGB, LiDAR, mmWave radar, and WiFi, under three settings and three protocols. Under random split (S1), LiDAR achieves 98.1, 94.9, and 92.5mm MPJPE for P1, P2, and P3, respectively, stably outperforming other modalities. The mmWave results are better than other modalities regarding the PA-MPJPE metric, achieving 55.6, 55.3, and 57.3mm PA-MPJPE for P1, P2, and P3, respectively. Due to the resolution limit of WiFi CSI, the results of WiFi modality are the worst. The RGB-based results are not satisfactory due to the domain gap, *i.e.*, the distribution shift between the dataset for the pre-trained model and our dataset.

Cross-Subject Results (S2). In S2, the focus of the evaluation is on testing the model’s robustness against subject differences. Results in Table 3 show that the LiDAR and mmWave radar models show good generalization ability under S2. The PA-MPJPE results of LiDAR and mmWave radar models only vary within 3mm when they are compared to the S1 for three protocols. Nevertheless, the 3D HPE model via WiFi CSI shows a significant decline in performance thanks to the limited resolution which fails to fully capture human subtle motions and differences, thereby restricting the model’s generalization ability across different subjects.

Cross-Environment Results (S3). In the cross-environment setting, the performances of all modalities significantly deteriorate. It is observed that 3D HPE based on mmWave radar achieves 166.2, 168.0, and 161.6mm MPJPE for P1, P2, and P3, respectively, significantly outperforming other modalities. A likely reason is that mmWave point cloud reflects the moving objects in space [32] and thus it is the least affected. The LiDAR MPJPE and PA-MPJPE drop a lot because the LiDAR data also captures many points on the ground and nearby objects. The WiFi CSI reflects the multi-path effect of the propagated signals, so the environment changes lead to decreasing performance for WiFi HPE model [58, 49].

		Protocol 1		Protocol 2		Protocol 3	
Modality	Setting	MPJPE (mm)	PA-MPJPE (mm)	MPJPE (mm)	PA-MPJPE (mm)	MPJPE (mm)	PA-MPJPE (mm)
RGB	S1	263.3	80.0	291.6	83.6	279.0	81.2
	S2	267.7	81.2	304.3	82.6	285.3	81.9
	S3	276.6	83.0	301.5	85.3	288.6	84.1
LiDAR	S1	98.1±2.2	65.2±0.7	94.9±1.1	60.4±1.8	92.5±0.6	61.5±1.3
	S2	110.1±2.9	66.2±1.2	103.9±0.6	60.3±2.3	103.8±1.5	61.5±1.2
	S3	192.3±30.4	100.4±5.4	186.0±2.9	103.5±11.9	303.8±11.6	133.0±3.3
mmWave	S1	109.8±2.7	55.6±1.4	124.3±2.2	55.3±2.2	117.0±3.7	57.3±1.8
	S2	128.4±6.9	58.7±4.3	142.2±0.6	57.4±2.3	129.7±2.2	60.0±1.7
	S3	166.2±4.5	73.9±2.7	168.0±0.9	73.0±3.9	161.6±1.8	73.7±0.6
WiFi	S1	186.9±0.1	120.7±0.9	213.5±0.5	121.4±0.1	197.1±0.6	121.2±0.5
	S2	222.3±0.8	125.4±2.3	247.0±0.2	122.7±1.3	231.1±0.4	124.0±0.5
	S3	367.8±0.9	121.0±2.2	360.2±1.3	117.2±0.9	369.5±0.3	116.0±1.8

Table 3: 3D human pose estimation results for RGB, LiDAR, mmWave radar, and WiFi. The mean and standard deviation of MPJPE are reported under 3 settings and 3 protocols.

		Protocol 1		Protocol 2		Protocol 3	
Modalities	Setting	MPJPE (mm)	PA-MPJPE (mm)	MPJPE (mm)	PA-MPJPE (mm)	MPJPE (mm)	PA-MPJPE (mm)
I+L	S1	94.3±1.5	63.9±0.6	90.1±1.8	58.9±2.1	87.5±0.8	59.8±1.2
	S2	109.4±1.6	65.8±0.6	103.5±0.6	60.2±2.4	104.6±0.6	62.1±0.3
	S3	159.6±25.9	84.5±1.8	153.5±3.37	87.1±10.3	192.1±21.8	89.6±3.9
R+W	S1	94.2±3.7	55.2±6.3	92.8±13.2	51.8±4.2	113.2±4.2	75.6±2.8
	S2	127.4±2.8	72.9±4.0	151.5±4.4	64.6±1.9	127.5±5.8	77.3±5.1
	S3	104.9±9.3	47.6±2.4	110.5±10.1	54.2±1.7	116.1±7.8	57.2±4.9
R+L+W	S1	74.1±1.7	46.7±1.4	72.7±6.8	42.7±1.1	72.7±6.8	42.7±1.1
	S2	111.9±3.6	83.0±3.6	106.5±1.1	63.5±2.2	99.6±1.5	72.0±1.5
	S3	119.0±3.8	66.8±5.8	111.1±7.8	61.8±6.8	126.3±17.9	61.0±10.8
R+L+W+I	S1	72.9±1.0	47.7±1.2	69.5±3.4	43.1±1.9	89.8±2.0	63.2±1.9
	S2	112.0±4.7	82.8±4.0	114.8±2.32	67.0±2.73	99.2±1.0	73.0±1.4
	S3	98.1±10.4	58.3±8.8	92.7±11.65	65.0±7.59	116.5±23.6	70.6±13.5

Table 4: 3D human pose estimation results of multi-sensor fusion, where the modalities are denoted as I (Image), L (Lidar), R (mmWave Radar) and W (WiFi CSI).

Modality Fusion. We search for the optimal weights and obtain the improved multi-modal HPE results in Table 4 compared to the single-modal results in Table 3. For example, the fusion of RGB images and LiDAR (I+L) outperforms LiDAR significantly for MPJPE under three settings. For all the activities (P3), the best PA-MPJPE results come from the modality fusion of R+L+W, achieving 42.7, 72.0, and 61.0mm for S1, S2, and S3 respectively. This demonstrates that in real-world scenarios, fusing multiple modalities in some ways for 3D HPE can be more robust and accurate.

6 Limitations of MM-Fi

The MM-Fi dataset currently has limitations regarding annotations and benchmarks. Firstly, the annotation process is manual and the quality is limited. Due to the resolution of wireless sensing data, the current sensing tasks are restricted to activity level and keypoint level, which have been validated with high quality. However, for tasks that require higher resolution, such as dense pose estimation, we only provide annotations obtained from algorithms that have not been validated. These annotations are included to facilitate new tasks and inspire further research. In the upcoming MM-Fi V2.0, we plan to use a motion capture system to annotate the dense pose to address this limitation. Secondly, as the first dataset to offer mmWave radar, LiDAR, RGBD, and WiFi data simultaneously, there are tasks that have not been extensively studied yet. Therefore, some baseline methods developed by us may not perform optimally without careful design. Our intention is to inspire researchers to explore these unexplored fields and contribute to the future benchmarking of the MM-Fi dataset. Thirdly, the current dataset is collected in a controlled condition, i.e., 3m away and same facing direction, with a single person. We plan to include multi-orientation, multi-location, and multi-user scenarios in MM-Fi 2.0. We acknowledge these limitations and aim to improve the dataset by addressing them in future versions. Our objective is to provide a comprehensive resource that encourages research and advancements in the non-intrusive wireless sensing research community.

7 Conclusion

In this paper, we present *MM-Fi*, a novel non-intrusive multi-modal 4D human pose dataset for wireless human sensing. It consists of four sensing modalities: RGB-D, LiDAR, mmWave radar, and WiFi, and is currently the most comprehensive benchmark for wireless human pose estimation. Our MM-Fi is composed of 320.76k synchronized frames, and 27 categories of poses performed by 40 subjects. The collection process and the four data modalities are introduced, followed by extensive experiments to produce a single-modal and multi-modal benchmark. Our proposed dataset contributes to the multi-modal human pose estimation research and helps researchers choose suitable sensor modalities according to their advantages and disadvantages. We hope that our proposed MM-Fi dataset and benchmarks can facilitate future research in machine learning, ubiquitous computing, computer vision, mobile computing, and healthcare.

Acknowledge. This work is supported by NTU Presidential Postdoctoral Fellowship, “Adaptive Multimodal Learning for Robust Sensing and Recognition in Smart Cities” project fund, at Nanyang Technological University, Singapore.

References

- [1] An, S., Li, Y., Ogras, U.: mri: Multi-modal 3d human pose estimation dataset using mmwave, rgb-d, and inertial sensors. arXiv preprint arXiv:2210.08394 (2022)
- [2] An, S., Ogras, U.Y.: Mars: mmwave-based assistive rehabilitation system for smart healthcare. *ACM Transactions on Embedded Computing Systems (TECS)* **20**(5s), 1–22 (2021)
- [3] An, S., Ogras, U.Y.: Fast and scalable human pose estimation using mmwave point cloud. arXiv preprint arXiv:2205.00097 (2022)
- [4] Andriluka, M., Pishchulin, L., Gehler, P., Schiele, B.: 2d human pose estimation: New benchmark and state of the art analysis. In: *Proceedings of the IEEE Conference on Computer Vision and Pattern Recognition*. pp. 3686–3693 (2014)
- [5] Antunes, J., Bernardino, A., Smailagic, A., Siewiorek, D.P.: Aha-3d: A labelled dataset for senior fitness exercise recognition and segmentation from 3d skeletal data. In: *BMVC*. p. 332 (2018)
- [6] Ar, I., Akgul, Y.S.: A computerized recognition system for the home-based physiotherapy exercises using an rgb-d camera. *IEEE Transactions on Neural Systems and Rehabilitation Engineering* **22**(6), 1160–1171 (2014)
- [7] Cai, Z., Ren, D., Zeng, A., Lin, Z., Yu, T., Wang, W., Fan, X., Gao, Y., Yu, Y., Pan, L., et al.: Humman: Multi-modal 4d human dataset for versatile sensing and modeling. In: *European Conference on Computer Vision*. pp. 557–577. Springer (2022)
- [8] Chen, A., Wang, X., Zhu, S., Li, Y., Chen, J., Ye, Q.: mmbody benchmark: 3d body reconstruction dataset and analysis for millimeter wave radar. In: *Proceedings of the 30th ACM International Conference on Multimedia*. pp. 3501–3510 (2022)
- [9] Chen, Y., Zhang, Z., Yuan, C., Li, B., Deng, Y., Hu, W.: Channel-wise topology refinement graph convolution for skeleton-based action recognition. In: *Proceedings of the IEEE/CVF International Conference on Computer Vision*. pp. 13359–13368 (2021)
- [10] Cong, P., Xu, Y., Ren, Y., Zhang, J., Xu, L., Wang, J., Yu, J., Ma, Y.: Weakly supervised 3d multi-person pose estimation for large-scale scenes based on monocular camera and single lidar. In: *Proceedings of the AAAI Conference on Artificial Intelligence*. vol. 37, pp. 461–469 (2023)
- [11] Dai, Y., Lin, Y., Lin, X., Wen, C., Xu, L., Yi, H., Shen, S., Ma, Y., Wang, C.: Sloper4d: A scene-aware dataset for global 4d human pose estimation in urban environments. In: *Proceedings of the IEEE/CVF Conference on Computer Vision and Pattern Recognition*. pp. 682–692 (2023)
- [12] Ding, G., Sener, F., Yao, A.: Temporal action segmentation: An analysis of modern technique. arXiv preprint arXiv:2210.10352 (2022)
- [13] Geng, J., Huang, D., De la Torre, F.: Densepose from wifi. arXiv preprint arXiv:2301.00250 (2022)
- [14] Ghorbani, S., Mahdavian, K., Thaler, A., Kording, K., Cook, D.J., Blohm, G., Troje, N.F.: Movi: A large multi-purpose human motion and video dataset. *Plos one* **16**(6), e0253157 (2021)

- [15] Güler, R.A., Neverova, N., Kokkinos, I.: Densepose: Dense human pose estimation in the wild. In: Proceedings of the IEEE conference on computer vision and pattern recognition. pp. 7297–7306 (2018)
- [16] Ionescu, C., Papava, D., Olaru, V., Sminchisescu, C.: Human3.6m: Large scale datasets and predictive methods for 3d human sensing in natural environments. *IEEE transactions on pattern analysis and machine intelligence* **36**(7), 1325–1339 (2013)
- [17] Jiang, W., Xue, H., Miao, C., Wang, S., Lin, S., Tian, C., Murali, S., Hu, H., Sun, Z., Su, L.: Towards 3d human pose construction using wifi. In: Proceedings of the 26th Annual International Conference on Mobile Computing and Networking. pp. 1–14 (2020)
- [18] Joo, H., Liu, H., Tan, L., Gui, L., Nabbe, B., Matthews, I., Kanade, T., Nobuhara, S., Sheikh, Y.: Panoptic studio: A massively multiview system for social motion capture. In: Proceedings of the IEEE International Conference on Computer Vision. pp. 3334–3342 (2015)
- [19] Kuehne, H., Richard, A., Gall, J.: A hybrid rnn-hmm approach for weakly supervised temporal action segmentation. *IEEE transactions on pattern analysis and machine intelligence* **42**(4), 765–779 (2018)
- [20] Lee, L.H., Braud, T., Zhou, P., Wang, L., Xu, D., Lin, Z., Kumar, A., Bermejo, C., Hui, P.: All one needs to know about metaverse: A complete survey on technological singularity, virtual ecosystem, and research agenda. *arXiv preprint arXiv:2110.05352* (2021)
- [21] Li, J., Zhang, J., Wang, Z., Shen, S., Wen, C., Ma, Y., Xu, L., Yu, J., Wang, C.: Lidarcap: Long-range marker-less 3d human motion capture with lidar point clouds. In: Proceedings of the IEEE/CVF Conference on Computer Vision and Pattern Recognition. pp. 20502–20512 (2022)
- [22] Li, Z., Abu Farha, Y., Gall, J.: Temporal action segmentation from timestamp supervision. In: Proceedings of the IEEE/CVF Conference on Computer Vision and Pattern Recognition. pp. 8365–8374 (2021)
- [23] Lin, T.Y., Maire, M., Belongie, S., Hays, J., Perona, P., Ramanan, D., Dollár, P., Zitnick, C.L.: Microsoft coco: Common objects in context. In: European conference on computer vision. pp. 740–755. Springer (2014)
- [24] Mehta, D., Rhodin, H., Casas, D., Fua, P., Sotnychenko, O., Xu, W., Theobalt, C.: Monocular 3d human pose estimation in the wild using improved cnn supervision. In: 2017 international conference on 3D vision (3DV). pp. 506–516. IEEE (2017)
- [25] Mehta, D., Sridhar, S., Sotnychenko, O., Rhodin, H., Shafiei, M., Seidel, H.P., Xu, W., Casas, D., Theobalt, C.: Vnect: Real-time 3d human pose estimation with a single rgb camera. *Acm transactions on graphics (tog)* **36**(4), 1–14 (2017)
- [26] Neverova, N., Novotny, D., Vedaldi, A.: Correlated uncertainty for learning dense correspondences from noisy labels. In: Advances in Neural Information Processing Systems (2019)
- [27] Nirmal, I., Khamis, A., Hassan, M., Hu, W., Zhu, X.: Deep learning for radio-based human sensing: Recent advances and future directions. *IEEE Communications Surveys & Tutorials* **23**(2), 995–1019 (2021)
- [28] Olivares, A., Górriz, J., Ramírez, J., Olivares, G.: Accurate human limb angle measurement: sensor fusion through kalman, least mean squares and recursive least-squares adaptive filtering. *Measurement Science and Technology* **22**(2), 025801 (2010)
- [29] Pavllo, D., Feichtenhofer, C., Grangier, D., Auli, M.: 3d human pose estimation in video with temporal convolutions and semi-supervised training. In: Conference on Computer Vision and Pattern Recognition (CVPR) (2019)
- [30] Pons-Moll, G., Baak, A., Helten, T., Müller, M., Seidel, H.P., Rosenhahn, B.: Multisensor-fusion for 3d full-body human motion capture. In: 2010 IEEE Computer Society Conference on Computer Vision and Pattern Recognition. pp. 663–670. IEEE (2010)
- [31] Quigley, M., Conley, K., Gerkey, B., Faust, J., Foote, T., Leibs, J., Wheeler, R., Ng, A.Y., et al.: Ros: an open-source robot operating system. In: ICRA workshop on open source software. p. 5. No. 3 in 2, Kobe, Japan (2009)
- [32] Rao, S.: Introduction to mmwave sensing: Fmcw radars. Texas Instruments (TI) mmWave Training Series pp. 1–11 (2017)

- [33] Ren, Y., Yang, J.: 3d human pose estimation for free-from and moving activities using wifi. arXiv preprint arXiv:2204.07878 (2022)
- [34] Ren, Y., Zhao, C., He, Y., Cong, P., Liang, H., Yu, J., Xu, L., Ma, Y.: Lidar-aid inertial poser: Large-scale human motion capture by sparse inertial and lidar sensors. *IEEE Transactions on Visualization and Computer Graphics* **29**(5), 2337–2347 (2023)
- [35] Sanakoyeu, A., Khalidov, V., McCarthy, M.S., Vedaldi, A., Neverova, N.: Transferring dense pose to proximal animal classes. In: *Proceedings of the IEEE Conference on Computer Vision and Pattern Recognition (CVPR)* (2020)
- [36] Sengupta, A., Jin, F., Zhang, R., Cao, S.: mm-pose: Real-time human skeletal posture estimation using mmwave radars and cnns. *IEEE Sensors Journal* **20**(17), 10032–10044 (2020)
- [37] Shahroudy, A., Liu, J., Ng, T.T., Wang, G.: Ntu rgb+ d: A large scale dataset for 3d human activity analysis. In: *Proceedings of the IEEE conference on computer vision and pattern recognition*. pp. 1010–1019 (2016)
- [38] Shi, L., Zhang, Y., Cheng, J., Lu, H.: Two-stream adaptive graph convolutional networks for skeleton-based action recognition. In: *Proceedings of the IEEE/CVF conference on computer vision and pattern recognition*. pp. 12026–12035 (2019)
- [39] Sun, K., Xiao, B., Liu, D., Wang, J.: Deep high-resolution representation learning for human pose estimation. In: *CVPR* (2019)
- [40] Von Marcard, T., Henschel, R., Black, M.J., Rosenhahn, B., Pons-Moll, G.: Recovering accurate 3d human pose in the wild using imus and a moving camera. In: *Proceedings of the European Conference on Computer Vision (ECCV)*. pp. 601–617 (2018)
- [41] Von Marcard, T., Pons-Moll, G., Rosenhahn, B.: Human pose estimation from video and imus. *IEEE transactions on pattern analysis and machine intelligence* **38**(8), 1533–1547 (2016)
- [42] Wang, Z., Gao, Z., Wang, L., Li, Z., Wu, G.: Boundary-aware cascade networks for temporal action segmentation. In: *Computer Vision–ECCV 2020: 16th European Conference, Glasgow, UK, August 23–28, 2020, Proceedings, Part XXV* 16. pp. 34–51. Springer (2020)
- [43] Xie, Y., Li, Z., Li, M.: Precise power delay profiling with commodity wifi. In: *Proceedings of the 21st Annual international conference on Mobile Computing and Networking*. pp. 53–64 (2015)
- [44] Xue, H., Ju, Y., Miao, C., Wang, Y., Wang, S., Zhang, A., Su, L.: mmmesh: Towards 3d real-time dynamic human mesh construction using millimeter-wave. In: *Proceedings of the 19th Annual International Conference on Mobile Systems, Applications, and Services*. pp. 269–282 (2021)
- [45] Yan, M., Wang, X., Dai, Y., Shen, S., Wen, C., Xu, L., Ma, Y., Wang, C.: Cimi4d: A large multimodal climbing motion dataset under human-scene interactions. In: *Proceedings of the IEEE/CVF Conference on Computer Vision and Pattern Recognition*. pp. 12977–12988 (2023)
- [46] Yang, J., Chen, X., Zou, H., Lu, C.X., Wang, D., Sun, S., Xie, L.: Sensefi: A library and benchmark on deep-learning-empowered wifi human sensing. *Patterns* **4**(3) (2023)
- [47] Yang, J., Zhou, Y., Huang, H., Zou, H., Xie, L.: Metafi: Device-free pose estimation via commodity wifi for metaverse avatar simulation. In: *IEEE World Forum on Internet of Things 2022* (2022)
- [48] Yang, J., Zou, H., Jiang, H., Xie, L.: Device-free occupant activity sensing using wifi-enabled iot devices for smart homes. *IEEE Internet of Things Journal* **5**(5), 3991–4002 (2018)
- [49] Yang, J., Zou, H., Zhou, Y., Xie, L.: Learning gestures from wifi: A siamese recurrent convolutional architecture. *IEEE Internet of Things Journal* **6**(6), 10763–10772 (2019)
- [50] Zhang, Z., Wang, C., Qin, W., Zeng, W.: Fusing wearable imus with multi-view images for human pose estimation: A geometric approach. In: *Proceedings of the IEEE/CVF Conference on Computer Vision and Pattern Recognition*. pp. 2200–2209 (2020)
- [51] Zhao, H., Jiang, L., Jia, J., Torr, P.H., Koltun, V.: Point transformer. In: *Proceedings of the IEEE/CVF international conference on computer vision*. pp. 16259–16268 (2021)
- [52] Zhao, M., Li, T., Abu Alsheikh, M., Tian, Y., Zhao, H., Torralba, A., Katabi, D.: Through-wall human pose estimation using radio signals. In: *Proceedings of the IEEE Conference on Computer Vision and Pattern Recognition*. pp. 7356–7365 (2018)

- [53] Zhao, M., Tian, Y., Zhao, H., Alsheikh, M.A., Li, T., Hristov, R., Kabelac, Z., Katabi, D., Torralba, A.: Rf-based 3d skeletons. In: Proceedings of the 2018 Conference of the ACM Special Interest Group on Data Communication. pp. 267–281 (2018)
- [54] Zheng, J., Shi, X., Gorban, A., Mao, J., Song, Y., Qi, C.R., Liu, T., Chari, V., Cornman, A., Zhou, Y., et al.: Multi-modal 3d human pose estimation with 2d weak supervision in autonomous driving. In: Proceedings of the IEEE/CVF Conference on Computer Vision and Pattern Recognition. pp. 4478–4487 (2022)
- [55] Zhou, X., Zhu, M., Leonardos, S., Daniilidis, K.: Sparse representation for 3d shape estimation: A convex relaxation approach. *IEEE transactions on pattern analysis and machine intelligence* **39**(8), 1648–1661 (2016)
- [56] Zhou, Y., Huang, H., Yuan, S., Zou, H., Xie, L., Yang, J.: Metafi++: Wifi-enabled transformer-based human pose estimation for metaverse avatar simulation. *IEEE Internet of Things Journal* (2023)
- [57] Zou, H., Yang, J., Prasanna Das, H., Liu, H., Zhou, Y., Spanos, C.J.: Wifi and vision multimodal learning for accurate and robust device-free human activity recognition. In: Proceedings of the IEEE/CVF conference on computer vision and pattern recognition workshops. pp. 0–0 (2019)
- [58] Zou, H., Yang, J., Zhou, Y., Xie, L., Spanos, C.J.: Robust wifi-enabled device-free gesture recognition via unsupervised adversarial domain adaptation. In: 2018 27th International Conference on Computer Communication and Networks (ICCCN). pp. 1–8. IEEE (2018)

A Appendix

A.1 Ethics Statement

The MM-Fi human subject study in this paper has been reviewed and approved by the IRB committee at the Nanyang Technological University (IRB-2022-1067). The MM-Fi data has been de-identified by facial blur. The subject recruitment is voluntary, and the involved subject has been informed that the de-identified data was made publicly available for research purposes. As far as we know, this research does not endanger any person directly. Nevertheless, it is acknowledged that pose estimation and activity recognition research can potentially be used with malicious intent, such as user behavior monitoring.

A.2 Dataset Documentation

Modality and Action Category. The MM-Fi dataset contains six modalities including RGB, infra, depth, mmWave, LiDAR and WiFi CSI with open and widely used data formats, and consists of 4 environments for domain diversity. Demonstration videos can be referred to our project page (<https://ntu-aiot-lab.github.io/mm-fi>). 40 volunteers participated in the data collection progress with 10 volunteers in one environment. The recommended actions contain daily actions and rehabilitation actions, which are summarized in Table 5. Besides, illustration of all actions by a volunteer can be viewed in the [action checklist](#) (*i.e.*, demo image sequence of each action).

Action	Description	Category	Action	Description	Category
A01	Stretching and relaxing	Rehabilitation activities	A15	Lunge (toward left)	Rehabilitation activities
A02	Chest expansion (horizontal)	Daily activities	A16	Lunge (toward right)	Rehabilitation activities
A03	Chest expansion (vertical)	Daily activities	A17	Waving hand (left)	Daily activities
A04	Twist (left)	Daily activities	A18	Waving hand (right)	Daily activities
A05	Twist (right)	Daily activities	A19	Picking up things	Daily activities
A06	Mark time	Rehabilitation activities	A20	Throwing (toward left)	Daily activities
A07	Limb extension (left)	Rehabilitation activities	A21	Throwing (toward right)	Daily activities
A08	Limb extension (right)	Rehabilitation activities	A22	Kicking (toward left)	Daily activities
A09	Lunge (toward left-front)	Rehabilitation activities	A23	Kicking (toward right)	Daily activities
A10	Lunge (toward right-front)	Rehabilitation activities	A24	Body extension (left)	Rehabilitation activities
A11	Limb extension (both)	Rehabilitation activities	A25	Body extension (right)	Rehabilitation activities
A12	Squat	Rehabilitation activities	A26	Jumping up	Rehabilitation activities
A13	Raising hand (left)	Daily activities	A27	Bowing	Daily activities
A14	Raising hand (right)	Daily activities			

Table 5: The action list including daily activities and rehabilitation activities.

Distribution and Maintenance. The dataset with recommended instructions on how to download and use is maintained in our GitHub repository (https://github.com/ybhbingo/MMFi_dataset) with a registered DOI, which we will update timely according to the users’ and community’s advice. In addition, for the accessibility of dataset and long-term preservation, we have uploaded dataset to Google Drive, Baidu Netdisk and Alibaba Cloud with long-term cloud storage service (links are shared in the GitHub repository). We provide two ways of downloading the dataset: whole zip file download and multi-split download. The original dataset is organized in a clear structure so that users could check the recovered dataset conveniently, which can be shown by Figure 4.

Modality	Data format	Data size	File extension	Modality	Data format	Data size	File extension
RGB	Numpy array	$297 \times 17 \times 2$.npy	WiFi CSI	MATLAB matrix	$297 \times 3 \times 114$.mat
infra1	Numpy array	$297 \times 17 \times 2$.npy	infra2	Numpy array	$297 \times 17 \times 2$.npy
mmWave	Binary	297 clouds	.bin	LiDAR	Binary	297 clouds	.bin
Depth	Image	$297 \times 640 \times 480$.png				

Table 6: The data formats for different modalities.

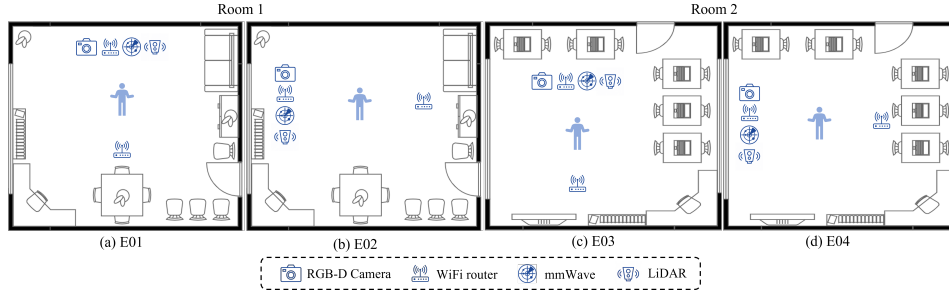


Figure 3: The illustration of the four environmental settings. The experiment is carried out in two rooms (Room 1 and Room 2), whose length and width are both 8.5m and 7.8m respectively.

Dataset Toolbox. For convenient data loading, we have transformed the sensing data from different modalities into the open and widely used data formats, which are listed in Table 6. We also developed the dataset toolbox in the GitHub repository (https://github.com/yhbbingo/MMFi_dataset) that provides the data loader for PyTorch deep learning framework. The users can download the data from the [link](#) and follow the instructions in our GitHub repository to load the data easily. The anonymized version of RGB images, preserving the identifiable information of volunteers (already with permissions from all volunteers), can be accessed after the [application forms](#).

Environmental Details. To enhance the diversity of the MM-Fi dataset, we acquired data from four distinct environmental settings (referred to as E01, E02, E03, and E04). Within each environment, a cohort of ten participants was enlisted to execute a series of 27 commonplace human activities. As shown in Fig. 3, the sensor platform is deployed both horizontally and vertically within Room 1 and Room 2, respectively, contributing to 4 environmental settings. While both rooms share identical dimensions (8.5 meters in length and 7.8 meters in width), they exhibit distinct spatial layouts, which leads to diverse and varied sensor signals.

Data Processing. It is worth noting that for modalities with fixed input size from sensors, we have reformed the sensing data into the common structured formats, i.e. an array structure in Numpy or MATLAB, as shown in Table 6. For LiDAR data, since the original point cloud contains redundant information (the laser scanner provides reflected data for all directions in our LiDAR device, Liu but we only focus on the areas of interests where the subject stands), we have filtered the whole cloud using bounding boxes. While for the mmWave modality, the number of points varies with the body movement, indicating that even two consecutive frames would likely have different data sizes. To enhance the sensing quality, we have aggregated five adjacent frames into a new frame for use. Furthermore, padding is adopted for mmWave and LiDAR point clouds produced by the PyTorch dataloader, in which the padded size is determined by the largest sample size within the batch. For WiFi CSI data, there are some “-inf” values in some sequences. The “-inf” number comes from the noise or empty frames from the CSI tool. In our benchmark, we deal with these numbers by linear interpolation. To facilitate the users, we have embedded these processing codes into our dataset tool. When the user loads our WiFi CSI data, these numbers will be handled by linear interpolation. The codes can be found [here](#).

Temporal Segment Annotation Process. As presented in Section 4.3, we provide the temporal segment labels to enable temporal action segmentation and to provide more fine-grained samples. The segment annotation process is performed by human annotators with an automated segment annotation program that feeds the human annotators with the long sequence frame-by-frame, and enables the generation of temporal segments through human selected breakpoints. Each breakpoint is essentially a frame that implies the end of an action. Each sequence is annotated by at least 5 human annotators. To ensure correct segment annotation, a voting process is performed after all human annotations are collected, where the breakpoints that are selected by the majority of the annotators are viewed as the ground-truth breakpoints. The resulting action segments are frames between each breakpoint. The resulting fine-grained samples are recorded in a “.csv” file with sample records as shown in Table 7. The records includes the Environment, Subject, Action, and Segments information, where the different segments are represented by the beginning and end frames.

Environment	Subject	Action	Segments
E01	S01	A02	1-24; 25-50; 51-78; 79-105; 106-132; 133-160; 161-188; 189-218; 219-247; 248-277; 278-297
E01	S03	A18	1-15; 16-28; 29-41; 42-54; 55-67; 68-82; 83-96; 94-110; 111-124; 125-139; 140-152; 153-167; 168-181; 182-196; 197-210; 211-225; 226-239; 240-254; 255-267; 268-282; 283-297

Table 7: The data formats for different modalities.

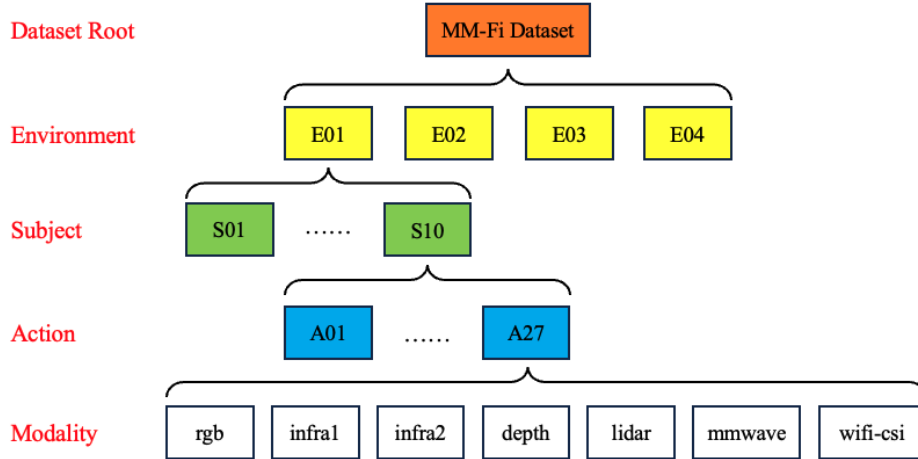


Figure 4: The expanded directory of original MM-Fi dataset.

Additional Annotator Details. Besides the regular loss function for annotating optimization, there usually exists body occlusion in a series of actions, which would cause failure of keypoints recognition and thus lead to inaccurate ground truth. As a result, we have introduced the specific regularizer \mathcal{L}_A for better annotation quality with expert knowledge from several action directors and volunteers. To be specific, we take the action "throwing toward left" (A20) for instance to illustrate how we define \mathcal{L}_A and handle the occlusion problem. When a volunteer faces toward the left side, the left part of the body (including the left arm and the left hip joint) would not be observed by the sensors, so we put more regularizer terms regarding the relative positions between the joints, which is denoted by:

$$\mathcal{L}_A = \sum_{n=1}^N \{ \gamma_1 \|d(p_{n,lp}, p_{n,rp}) - l_p\| + \gamma_2 \|d(p_{n,ls}, p_{n,rs}) - l_s\| + \gamma_3 h(p_n) \}, \quad (3)$$

where $p_{n,lp}$ and $p_{n,rp}$ denote the left and right hip joint of n th frame, respectively. l_p is the mean hip distance for the specific volunteer. The first term in (3) regularizes the unobservable left hip. Similarly, the second term is designed for the unobservable shoulder joint. The last term plays the role of constraining all the joints so that they would be within the sensing area, and the arms and legs would not be "bent" backward given the particular coordinates.

A.3 License Agreement

This work has been licensed under [CC BY-NC 4.0](#), and we bear all responsibility in case of violation of rights, the novelty of work, and privacy leaks.

A.4 Benchmark Implementation Details

We implemented all the baseline methods using the PyTorch framework and ensured that the hyperparameter settings matched those specified in the original papers. All the codes with a manual (README) for benchmarking each modality can be checked in the [link](#). To account for variability, we conducted each experiment three times with different random seeds and reported the mean and standard deviation of the results. Our experiments were performed on a local Ubuntu 20.04 server equipped with 4 NVIDIA RTX 3090 GPUs, an AMD Ryzen PRO 3000WX Series Processor (64 Cores), and 128GB RAM. The learned weights for multi-modal fusion are summarized in Table 8.

A.5 Details of Baseline Models.

WiFi We utilize MetaFi++ as our baseline, which is based on a convolutional network and employs a self-attention mechanism (in transformer) to learn the importance between different antennas. This enables selective fusion of relevant information from antennas, resulting in enhanced spatial capture capability and achieving state-of-the-art scores. There are approaches in the field of WiFi pose estimation, e.g., GoPose, WiPose, and Winect, all of which only use convolutional methods. Moreover, these methods handle WiFi data with only 30 subcarriers, while our MM-Fi has a higher granularity of data with 114 subcarriers, so the inconsistency of data prevents us from using these methods as baselines.

LiDAR and mmWave radar The current human pose estimation (HPE) methods for point cloud consist of convolutional networks, graph neural network, and the recent transformer. We chose Point Transformer [1] as our point cloud backbone because it shows state-of-the-art performance on many point cloud recognition tasks. Its design utilizes the self-attention mechanism to minimize the computational complexity for each layer and maximize the number of parallelizable calculations, which perfectly matches the characteristic of point cloud data.

RGB The visual baseline (VideoPose3D) is a popular 2D-to-3D solution that transforms 2D keypoints to the 3D keypoints, developed by Facebook Research. We choose this baseline since it has been widely utilized in many human pose estimation benchmarks [1][2]. There are many other works in computer vision for 3D human pose estimation, and we welcome the community to supplement more benchmarking results on our dataset.

		Protocol 1	Protocol 2	Protocol 3
Modalities	Setting	weights	weights	weights
I+L	S1	[0.0432, 0.9568]	[0.0553, 0.9447]	[0.0614, 0.9386]
	S2	[0.0131, 0.9869]	[-0.0013, 1.0013]	[-0.0230, 1.0230]
	S3	[0.2634, 0.7366]	[0.2727, 0.7273]	[0.4957, 0.5043]
R+W	S1	[0.7955, 0.2045]	[1.0126, -0.0126]	[0.8197, 0.1803]
	S2	[0.9617, 0.0383]	[0.8124, 0.1876]	[0.9287, 0.0713]
	S3	[0.8786, 0.1214]	[0.9459, 0.0541]	[0.9166, 0.0834]
R+L+W	S1	[0.2146, 0.8506, -0.0652]	[0.2251, 0.7902, -0.0053]	[0.2251, 0.7802, -0.0053]
	S2	[0.1494, 0.9645, -0.1139]	[0.2251, 0.7802, -0.0053]	[0.0664, 0.9434, -0.0098]
	S3	[0.4307, 0.7733, -0.2040]	[0.7483, 0.3627, -0.1110]	[0.8843, 0.1852, -0.0695]
R+L+W+I	S1	[0.1391, 0.9152, -0.0913, 0.0370]	[0.1569, 0.8247, -0.0240, 0.0424]	[0.0822, 0.9123, -0.0550, 0.0605]
	S2	[0.1266, 0.9721, -0.1256, 0.0269]	[0.0529, 0.9523, 0.0618, -0.0670]	[0.0877, 0.9384, -0.0363, 0.0102]
	S3	[0.2319, 0.5135, 0.0378, 0.2167]	[0.3965, 0.4997, -0.0761, 0.1799]	[0.4144, 0.3995, -0.1052, 0.2913]

Table 8: The weight matrix for the multi-modal human pose estimation results. The weight order in the weights column corresponds to that in the modalities column.

A.6 Additional Evaluation of RGB Model

Due to the difference of viewing angles between the Human3.6M [16] and our dataset, the pre-trained model on Human3.6M does not achieve satisfactory performance on the MPJPE metric, though the PA-MPJPE is significantly reduced due to the coordinates alignment. For better evaluation of the MM-Fi’s RGB modality, the VideoPose3D [29] model has been further trained from scratch based on the MM-Fi’s RGB modality. To be detailed, we use 81 2D-keypoint frames to generate one 3D-joint frame on the equivalent of a padding size of 40. The Adam optimizer is adopted and the learning rate decays from 0.001 gradually along epochs. The results are summarized in Table 9. We can observe that the re-trained RGB model obtains the best performance compared to other modalities.

Setting	Protocol 1		Protocol 2		Protocol 3	
	MPJPE (mm)	PA-MPJPE (mm)	MPJPE (mm)	PA-MPJPE (mm)	MPJPE (mm)	PA-MPJPE (mm)
S1	64.7±0.5	34.8±0.1	68.5±1.4	31.5±0.1	60.5±0.4	32.5±0.2
S2	88.4±1.1	35.8±0.1	82.8±1.5	32.1±0.1	85.7±0.5	33.4±0.1
S3	104.8±0.7	40.4±0.1	82.8±1.5	32.1±0.1	85.7±0.5	33.4±0.1

Table 9: The performance of the re-trained RGB model on the MM-Fi dataset. The mean and standard deviation of MPJPE are reported under 3 settings and 3 protocols.

A.7 Visualization

To intuitively show the HPE results of each modality, we visualize the results of HPE using four modalities in Figure 5. It is shown that the results of RGB, LiDAR, and mmWave radar are quite accurate, but WiFi-based HPE is not satisfactory due to the resolution limitation.

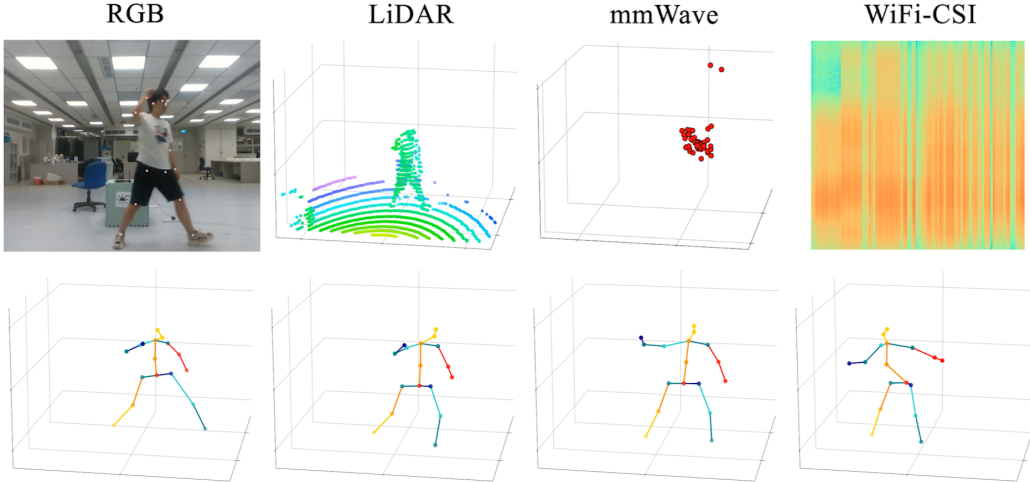


Figure 5: The visualization of human pose estimation using four modalities.

A.8 Benchmark on Skeleton-Based Action Recognition

The MM-Fi can also serve the skeleton-based action recognition task based on various data modalities. Here we leverage the results obtained by human pose estimation to conduct a new benchmark.

Implementation Details. In the official split of HPE, we have 30 subjects for training and 10 subjects for testing. After HPE, we have 3D human joints of 10 subjects, which serve as the dataset for skeleton-based action recognition using various data modalities. Each sequence is divided by 30 frames to generate small clips for action recognition. We split the data into 7 subjects (11340 frames) for training and 3 subjects (4860 frames) for testing. We leverage two novel skeleton-based action recognition methods, AGCN [38] (CVPR'19) and CTRGCN [9] (CVPR'21), with their pre-trained model parameters on NTU-RGBD datasets. The hyper-parameters for training follow the original papers. The learning rate starts from 0.1 and decays by 10 at the 5th and 10th epochs. The models are optimized by the SGD optimizer with a Nesterov momentum of 0.9. The models are trained for 20 epochs with a batch size of 32 and a weight decay of 0.0001.

Results. As shown in Table 10, we can see that both AGCN and CTRGCN perform the best using RGB data since the two models are originally built upon RGB data and the human joints predicted by RGBD are quite well in the manuscript (Table 3). The second best modality is the mmWave radar point cloud, which is better than the LiDAR results. However, in Table 3 of the manuscript, it is shown that the HPE results of LiDAR are better than those of mmWave. We think that the better action recognition results of mmWave are caused by a more smooth prediction of sequences. The WiFi data cannot enable action recognition, as we find that some frames of joints predicted by WiFi are not robustly consistent. Another interesting finding is that CTRGCN performs better than AGCN on public RGBD datasets, but for various data modalities in MM-Fi, AGCN performs better. This implies that CTRGCN overfits some RGBD datasets and may not really generalize well on other datasets.

A.9 More Uses: New Research Tasks

MM-Fi significantly expands the horizons of research by furnishing meticulously synchronized multimodal human sensing data. As advised by the reviewer, we have encapsulated these novel research directions as follows, and have incorporated these enhancements into the manuscript:

	AGCN [38]		CTRGCN [9]	
	Top 1 (%)	Top 5 (%)	Top 1 (%)	Top 5 (%)
WiFi	5.45	21.63	5.12	23.33
mmWave Radar	65.25	93.44	60.97	91.07
LiDAR	54.44	91.03	35.97	74.12
RGBD	87.78	99.42	66.98	93.60

Table 10: The benchmark results for skeleton-based action recognition.

Cross-domain wireless sensing. The realm of wireless sensing is often challenged by recognition performance disparities stemming from domain shifts, which arise due to variations in environments and subjects. While this issue has garnered extensive exploration within action recognition based on RGB data, it remains relatively uncharted within the context of Human Pose Estimation (HPE) utilizing modalities such as mmWave, LiDAR, and WiFi. The MM-Fi dataset presents a unique opportunity to address this gap by facilitating research into domain adaptation and generalization for HPE on these emerging modalities. By enabling investigations into the adaptation of models across diverse domains, MM-Fi opens avenues for enhancing the robustness and applicability of wireless sensing technologies.

Cross-modal supervision for fine-grained wireless sensing. Previous works have showcased the utility of WiFi and mmWave radar for action recognition tasks. However, MM-Fi introduces a transformative dimension by offering meticulously synchronized multimodal data and comprehensive annotations. Based on MM-Fi, cross-modal learning can enable these sparse data modality to achieve fine-grained recognition tasks, e.g., human pose estimation and action segmentation.

Multi-modal wireless sensing. MM-Fi’s integration of five distinct modalities empowers researchers to explore the potential of multi-modal wireless sensing, where different sensing technologies complement each other to achieve more comprehensive and accurate insights into human behavior. For example, integrating RGB and WiFi can overcome the illumination issue of RGB-based solutions. This dataset serves as a launchpad for pioneering investigations into techniques that fuse information from LiDAR, mmWave radar, and WiFi signals to attain a holistic understanding of human actions and interactions. As researchers delve into multi-modal fusion methods, the MM-Fi dataset becomes a valuable resource for the development of advanced solutions that leverage the strengths of each modality, while compensating for their individual limitations.

A.10 Sensor Specifications

We briefly introduce the sensors used in our collection platform. Note that some sensors have very high sampling rate or data resolution, but we do not use the maximum setting in our data collection. The experimental setting has been illustrated in Section 3.

WiFi We develop a customized OpenWrt firmware for COTS WiFi devices (TP-Link N750) using the Atheros CSI tool to enable a large-scale implementation of various CSI-enabled applications. Our platform reports all the 114 subcarriers for the 40 MHz bandwidth on each antenna pair operating on 5 GHz. The platform has 3 pairs of antennas with one on transmitter and three on receivers to collect the CSI data based on our developed firmware tool, which finally provides a CSI data stream of 100Hz after average sliding on the raw data.

Lidar Ouster OS1 32-channel LiDAR is used to acquire dense point cloud data. It contains 32 vertical beams, which provides ± 0.7 -5cm vertical angular resolution. Its vertical field of view is 45 degrees and its range is 120m. It can capture dense point clouds with a maximum of 1,310,720 points per second. In MM-Fi, we collected the raw data under 10 Hz frequency.

mmWave radar The Texas Instruments (TI) IWR6843AOP mmWave radar is used to collect mmWave point clouds with up to 30FPS. It is an integrated single-chip mmWave sensor that has 3 antennas to transmit FMCW and use 4 antennas to receive reflected FMCW by utilizing 60-64 GHz radio band. Under the condition of 1.0-V internal LDO bypass model and 48% duty cycle, its typical power consumption is 1.75 W.

RGB-D The Intel RealSense camera D435, consisting of a depth module, an RGB module and a Realsense vision processor D4, is a stereo solution, offering quality depth for a variety of applications.

The RGB module applies the rolling shutter technology, enabling the maximal 1920x1080 high-resolution RGB frame acquisition at a sensing rate of 30 fps. Its horizontal and vertical fields of view are 69 degrees and 42 degrees, respectively. The depth module, formed with one IR projector and two imagers, could obtain a larger sensing field of view with 87 (horizontal) and 58 (vertical) degrees, and provide a 1280x720 resolution depth frame at up to 90 fps. What's more, due to the global shutter technology, the depth module could even work in low-light situations, making the Realsense D435 a good solution for all-day depth sensing applications.